Industrial Chemistry & Materials

ROYAL SOCIETY OF CHEMISTRY

PAPER

View Article Online
View Journal | View Issue

Cite this: *Ind. Chem. Mater.*, 2023, **1**, 117

Co and Ni single sites on the $(111)_n$ surface of γ-Al_2O_3 – a periodic boundary DFT study†

Jiande Gu,* Jing Wang and Jerzy Leszczynski *

The influences of increasing the number of d-electrons in the single metal (Fe-like) substituted $(111)_n$ surface of γ-Al_2O_3 on its possible catalytic effects were explored. The energetic properties, local structures, and in-site electron configurations of the most active tri-coordinated Co and Ni single-site $(111)_n$ surface of γ-Al_2O_3 have been studied using the density functional theory (DFT) approach under periodic boundary conditions. The replacement of Al by a Co or Ni atom on the I position of the $(111)_n$ surface leads to significant elongations of metal–O distances. The energy released from the substitution process on the Al_I site of the $(111)_n$ surface follows the sequence Ni_I (164.85 kcal mol^{-1}) > Co_I (113.17 kcal mol^{-1}) > Fe_I (44.30 kcal mol^{-1}). The triplet and quintet (ground state) of the Co_I substituted complex are energy degenerate. Also, the doublet and quartet (ground state) of the Ni_I substituted complex have the same stable energy. This energy degeneracy comes from the α–β electron flipping on the p-orbital of the neighboring O that is next to the substituted Co_I or Ni_I site on the $(111)_n$ surface of γ-Al_2O_3. Different from the Fe_I substituted single-site $(111)_n$ surface, in which the electron configuration of Fe_I varies according to its spin-multiplicity state, substituted Ni_I has a unique d^8 electron configuration in all three spin states, and similarly, Co_I has a unique d^7 electron configuration in all three open shell spin states. An increase of the population of d-electrons in the single metal substituted $(111)_n$ surface of γ-Al_2O_3 is likely to provide a more stable electron configuration in the metal catalytic center.

Keywords: Co substituted surface of γ-Al_2O_3; Ni substituted surface of γ-Al_2O_3; $(111)_n$ surface; Periodic boundary DFT approach; Metal catalytic center.

Received 3rd November 2022,
Accepted 5th January 2023

DOI: 10.1039/d2im00039c

rsc.li/icm

1 Introduction

Single metal atoms have been widely applied and extensively advanced in catalytic processes.[1–21] Surface-supported single-site metal atoms have wide-ranging applications in important chemical processes such as catalyzing the oxidation of CO,[1,5–17] in reforming reactions,[18,19] and in generating biofuels and biomass-derived chemicals by conversion of oxygen-rich biomass through hydro-deoxygenation processes.[20] ZnO surface supported single Pt and Au atom-centers have exhibited remarkable catalytic activity for reformation of methanol to H_2 and CO_2.[18] Catalysts with Fe deposited on SiO_2 surfaces have been demonstrated to have notable activity and selectivity for direct nonoxidative conversion of methane.[21] Heterogeneous catalysts such as single site Pd species framed in mesoporous organosilica have been effectively used for oxidative Heck reaction[22] and a single site Ni-modified Zn-MOF has been exemplified to have high selectivity for dimerization of ethylene.[23] A series of transition metal single-atom catalysts (*i.e.*, Co, Ni, Fe, Mn, Cu) has been developed. Extensive research on Ni-based and Co-based single-atom catalysts resulted in various applications in electro- and photocatalysis, batteries, solar cells, natural gas conversion, oxidations, hydrogenations, and dehydrogenation reactions.[24]

Alumina (Al_2O_3) has been recognized as a promising support for single-site atom catalysts.[1–6,16,17] As an effective support, Al_2O_3 has the function of stabilizing single atoms and even improving the catalytic activities and the selectivity of these single site atoms in catalytic processes.[16,17,25–30] Gamma-alumina (γ-Al_2O_3) is one of the important phases of this oxide. It has been well established and widely applied in experimental investigations.[31,32] Routinely, γ-Al_2O_3 has been defined as a defective spinel structure in which Al vacancy sites are distributed within the lattice.[32–34]

Both experimental modeling and theoretical modeling on low-index surfaces indicate that penta-coordinated Al sites[26,27,29,30,35,36] and tri-coordinated Al centers on the

Interdisciplinary Nanotoxicity Center, Department of Chemistry, Physics and Atmospheric Sciences, Jackson State University, Jackson, MS 39217, USA.
E-mail: jiande@icnanotox.org, jerzy@icnanotox.org

† Electronic supplementary information (ESI) available. See DOI: https://doi.org/10.1039/d2im00039c

surfaces are especially important in the formation of active centers of catalysts.[25,30,34,37–43] The highly reactive acid–base pairs created at the tri-coordinated Al on the γ-Al_2O_3 surfaces enable low-energy pathways for the heterolytic splitting of C–H bonds of methane.[37,38] Recent studies have demonstrated that the most stable (110) surface of γ-Al_2O_3 provides three tetra-coordinated Al/Fe sites and one tri-coordinated Al/Fe site. On the other hand, a newly uncovered form of the (111) surface of γ-Al_2O_3 provides support for three structural stable tri-coordinated single Al/Fe sites on the γ-Al_2O_3 surface.[30,44]

The catalytic characteristics of single metal atoms on various supporting backgrounds have been reported to be very sensitive to the electronic and geometric surroundings of the support.[45] The electronic structures of single-atom sites can be affected by the interacting atoms encircled, which might lead to alternations in the catalytic behaviors as compared to single-atom sites on nonmetallic supports.[45–54] The variation of electronic and geometric surroundings of supports can provide new perceptions for activity and selectivity as well as for catalyzing effects.

As an elaboration of our recent studies on the formation of γ-Al_2O_3 supported tri-coordinated Fe single-site complexes,[29,30] here we report the results of computational investigations on the local coordination and the in-site electronic structures of the Co and Ni single-atom sites on the most active tri-coordinated Al/Fe single-site (111) surface of γ-Al_2O_3. Compared to that of Fe, the electronic structures of the related Co and Ni compounds increase the population of d-electrons by 1 (Co) and 2 (Ni), respectively. Therefore, a theoretical investigation of these systems enables the elucidation of the effects of variations of d-electron population on their energetic properties and their microstructural characteristics. Such studies can provide a deep-rooted understanding and new outlooks for the activities, selectivity, and possible catalytic effects of these γ-Al_2O_3 supported single-atom metal systems.

2 Results and discussion

2.1 Co single site on the $(111)_n$ surface of γ-Al_2O_3

Among three different Al sites exposed on the $(111)_n$ surface (M_I, Al_{II}, and Al_{III} as shown in Fig. 1), M_I has been recognized to be the most stable site to host Fe in a previous study.[30] The energy released from this most stable substitution Fe^{3+} (sextet) + [$(111)_n$ surface of γ-Al_2O_3] → Al^{3+} + [Fe_I (doublet) on the $(111)_n$ surface of γ-Al_2O_3] has been calculated to be −44.30 kcal mol^{-1}. This provides an additional (by about 22.82 and 26.56 kcal mol^{-1}, respectively) energy gain compared to predictions for the two other possible Fe replaced sites for the ground state.[30] Consequently, this most stable substitution site is our focal point for the present research.

In this study, the spin multiplicity of Co was considered to vary from singlet (with $2S + 1 = 1$) to triplet, quintet, and septet, respectively. The quintet ($2S + 1 = 5$) has been found to be the ground state for the Co replacements on the Al_I site of the $(111)_n$ surface of γ-Al_2O_3. The energy released from this Co substitution process Co^{3+} (quintet) + [$(111)_n$ surface of γ-Al_2O_3] → Al^{3+} + [Co_I (spin-state) on the $(111)_n$ surface of γ-Al_2O_3] has been computed to be −113.17 kcal mol^{-1} for the quintet, about −68.87 kcal mol^{-1} higher than the energy gain in the corresponding Fe substitution. The relative stable energies of the Co_I substituted surface $(111)_n$ of gamma alumina with different spin states are summarized in Table 1. It is important to note that the triplet is virtually the same as the quintet in terms of energy. The ground state is therefore degenerate. Since the energy difference between ion Co^{3+} (quintet, ground state) and ion Co^{3+} (triplet) amounts to 44.33 kcal mol^{-1} in the present calculation, this degeneracy of the γ-Al_2O_3 supported Co_I complex implies that the coordination of the γ-Al_2O_3 surface may affect the peripheral electronic structure around the hosted Co^{3+}.

2.1.1 Local structure Co_I site on the $(111)_n$ surface. The coordinates of the optimized structures of the Co_I substituted $(111)_n$ surface of the supercell in the singlet, triplet, quintet, and septet states are listed in the ESI.†

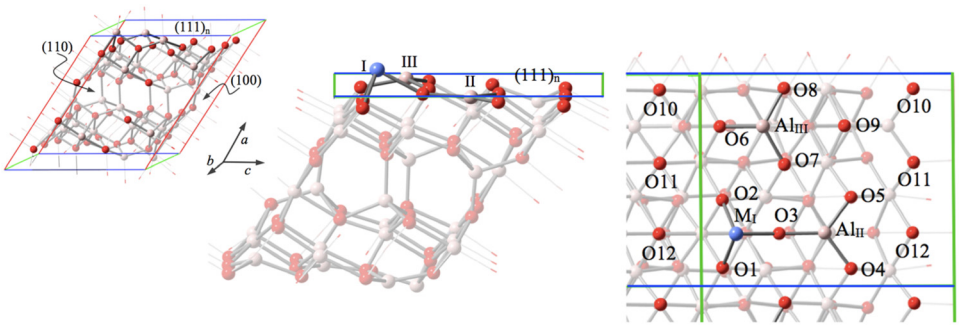

Fig. 1 The fully optimized supercell (left) and the $(111)_n$ surface structure (side view and top view). The supercell model consists of two units along the $(111)_n$ surface direction (8 atomic slabs) adopted in this study. The upper $(111)_n$ surface layer consists of three metal atoms (M_I, Al_{II}, and Al_{III}, where M_I represents Al, Co, and Ni) and 12 oxygen atoms. The bottom $(111)_n$ surface layer consists of three Al atoms (Al_I, Al_{II}, Al_{III}) and 12 oxygen atoms. Color legend: red for O, light pink for Al, and blue for Co or Ni.

Table 1 Relative energy of the Co_I substituted surface $(111)_n$ of gamma alumina, optimized using the MN12-L functional with basis sets SV[a]

Site	Singlet	Triplet	Quintet	Septet
Co_I	6.165	0.004	0.000	12.919

[a] For site labels, see Fig. 1. Relative energy in kcal mol^{-1}.

Table 2 displays the main geometric parameters of the optimized structure of the Co_I substituted $(111)_n$ surface of the supercell. Replacement of Al_I by Co on the $(111)_n$ surface results in elongations of metal–O bond lengths, especially for the high spin states, as compared to the pure γ-Al_2O_3. The Co_I–O distances amount to 1.93–1.95 Å for the ground state (quintet) of the Co_I substituted $(111)_n$ complex, about 0.18 Å longer than the corresponding Al_I–O distance for the un-substituted $(111)_n$ surface. Coherent to the energetic degeneracy, nearly the same Co_I–O distances (1.93–1.95 Å) are identified for the corresponding triplet state. A similar local structure is also unveiled for the system with the highest spin state. The related Co_I–O distances are predicted to be 1.94–1.95 Å for the septet state. On the other hand, the Co_I–O distances are around 1.77–1.78 Å for the low spin state (singlet) of the Co_I substituted $(111)_n$ surface of γ-Al_2O_3, ~0.01 Å longer than the corresponding Al_I–O distance of the un-substituted $(111)_n$ surface only. The Co_I–O bond distances are strongly correlated to the spin multiplicity of the coordinated Co on the $(111)_n$ surface of γ-Al_2O_3. This M_I–O bond distance–spin multiplicity correlation can also be found in the Fe_I substituted $(111)_n$ surface of γ-Al_2O_3, in which the Fe_I–O bond distances are reported to be around 1.78 Å for the low-spin state (doublet) and 1.91–1.94 Å for the high-spin states (quartet and sextet), accordingly.

2.1.2 Electron density distribution, DOS, and MO analysis of the Co_I site. The substitution of Co on the Al_I site leads to charge redistributions of the surrounding O atoms as revealed by the Mulliken population analysis (Table 3). The charge on the Co_I atom is 1.471 au in the singlet state. In comparison with the Al_I atom, Co_I charged on the $(111)_n$ surface is reduced by about 0.30 au. Consequently, the O atoms coordinated to the Co_I are expected to be less charged, as compared to the non-substituted complex in the low-spin state. The charge densities on the O1 and O2 atoms are calculated to be −1.056 and −1.052 au, while these charges amount to −1.216 au on the non-substituted surface. Also, the charge density on O3 is −1.099 au, which is smaller by 0.07 au in comparison with the non-substituted surface (−1.169 au). In the high spin states, the charge and spin density distributions are similar among these three states. For the Co_I site, the charge amounts to 1.547 au and the spin density amounts to 2.72 and for all three coordination O sites, the charges are approximately −1.21 au and the spin densities are approximately 0.08. Therefore, for the open-shell system, the variation of the total spin density does not alter the local electronic structure of the Co_I coordination site. Roughly, three spin electrons can be assigned to the Co_I site, while one can be allocated to the neighboring O12 site of the surface layer (spin density of 0.72, β-spin in the triplet and 0.72, α-spin in the quintet). For the septet state, one more spin electron is redistributed on the un-substituted $(111)_n$ surface.

For the singlet state, the analysis of the projected density of states (PDOS, Fig. 2) reveals the typical closed-shell character, with symmetric α–β spin density of states.

While the unoccupied states closest to the band gap are mainly determined by the d-orbitals of the coordinated Co atom, the occupied states near the band gap are dominated by the orbitals of the O atoms in the surface layer. The band gap (HOMO–LUMO gap) is predicted to be 0.49 eV for the singlet state of the Co_I substituted $(111)_n$ surface system. This band gap is about 0.17 eV smaller than that of the un-substituted $(111)_n$ surface of γ-Al_2O_3 (0.66 eV).[30,44] As a comparison, the minimum direct band gap (β-spin) for the doublet state of the Fe_I substituted $(111)_n$ surface was reported to be 0.47 eV.[30]

The corresponding MO analysis reveals that the p-type orbitals of O12 of both Co_I substituted and un-substituted (the bottom layer of the supercell in Fig. 3 of the HOMO) surfaces dominate the HOMO. Thus, the HOMO is not localized entirely around the metal supporting site; it spreads to both substituted and the un-substituted surfaces.

Three fully occupied d-orbitals of Co_I have been identified to contribute to the HOMO−32 and molecular orbitals below. These occupied d-type related MOs are highly non-localized. In contrast, the LUMO (also LUMO+1) is well localized on the d-type orbital of the surface coordinated Co_I and the p-orbital of the related supporting O atoms. Hence, these two d-orbitals of Co_I are totally unoccupied. On the $(111)_n$ surface, the supported Co_I has the closed-shell d^6 electron configuration in the singlet state.

Table 2 Geometries of the local structure of the Co_I substituted surface $(111)_n$ of gamma alumina, optimized using the MN12-L functional with basis sets SV[a]

	Non-substituted	Co-substituted			
	Singlet	Singlet	Triplet	Quintet	Septet
RI-1	1.766	1.772	1.946	1.947	1.942
RI-2	1.767	1.774	1.948	1.948	1.945
RI-3	1.763	1.778	1.929	1.932	1.939
D1123	51.29	58.10	57.97	58.10	58.36

[a] RI-*i*: Co–O atomic distance for substituted surfaces (Al–O atomic distance for non-substituted surface) in Å; D*ijkl*: dihedral angle in (°); for labels, see Fig. 1.

Table 3 Mulliken charge and spin density of the local structure of the Co_I substituted surface $(111)_n$[a]

	Singlet		Triplet		Quintet		Septet	
	Charge	Spin	Charge	Spin	Charge	Spin	Charge	Spin
Co_I	1.4711 (1.7668)	0.000 (0.000)	1.5467	2.724	1.5463	2.724	1.5478	2.724
O1	−1.0557 (−1.2165)	0.000 (0.000)	−1.2100	0.076	−1.2096	0.081	−1.2117	0.082
O2	−1.0517 (−1.2158)	0.000 (0.000)	−1.2082	0.076	−1.2080	0.081	−1.2097	0.082
O3	−1.0992 (−1.1686)	0.000 (0.000)	−1.1853	0.073	−1.1855	0.073	−1.1905	0.071
O12	−1.1294	0.000	−0.8021	−0.721	−0.8024	0.724	−0.7957	0.731

[a] Analysis based on the density calculated using the MN12-L functional with basis set SV. For labels, see Fig. 1. The numbers in the parentheses are for the Al_I site in the non-substituted system.

Consistent with the charge and spin density distributions, the PDOSs of the high spin states exhibit nearly the same band character of the coordinated Co_I for both triplet and quintet states. A similar feature is also shown in the band of the septet state. There are no contributions near the band gap from the d- or s-orbitals of the γ-Al_2O_3 surface supported Co_I for these high spin states (Fig. 4).

The state densities closest to the band gap are mainly determined by the sp^3-orbitals of Al of the un-substituted $(111)_n$ surface and the p-orbitals of the O atoms in the surface layer. The band gaps (HOMO–LUMO gap) are evaluated to be 0.47 eV (α-spin) and 0.66 eV (β-spin) for the triplet state, and 0.66 eV (α-spin) and 0.48 eV (β-spin) for the quintet state, respectively. A large band gap is found for the α-spin contribution in the septet state. For this state, the band gap is 1.76 eV for α-spin and 0.65 eV for the β-spin part. Interestingly, the band gap for the highest spin state (sextet) of the Fe_I substituted $(111)_n$ surface was reported to be 0.66 eV for α-spin and 0.27 eV for β-spin.[30] Taking into account that the s-type orbital (4s) of Co dominates the LUMO in the α-spin part for the septet state, this significant variation in the band gap is expected.

MOs of the triplet and quintet states depicted in Fig. 5 reveal the considerable similarity between the nearly degenerate triplet and quintet states. The sole difference is the components of the corresponding LUMO. In the triplet state, the p-type orbital with α-spin of O12 of the Co_I substituted surface is the main contribution of the LUMO with α-spin, while in the quintet state, it mainly arises from the LUMO with β-spin. The former suggests that in the triplet state the corresponding β component of the p-type orbital is occupied (providing a spin density of −0.72, and as a result of balancing 2.72 of spin density on Co, the total spin density amounts to 2). The latter implies that in the quintet, the α-spin component of this p-type orbital is occupied (the resulting spin density amounts to 0.72, leaving the corresponding β-spin orbital un-occupied). The energy degeneracy of the triplet and quintet states is due to this α–β electron flipping on the p-orbital of O12.

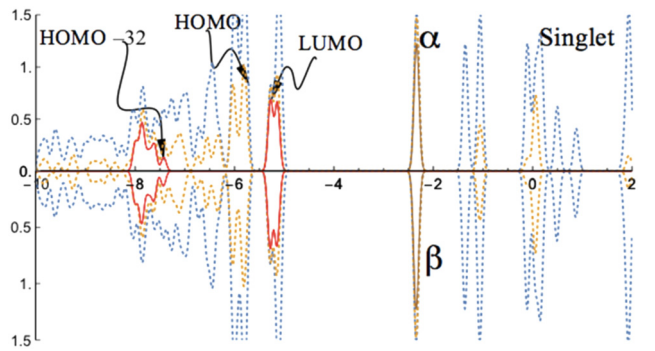

Fig. 2 PDOS of the Co_I substituted $(111)_n$ surface phase of γ-Al_2O_3 in the singlet state. The surface layer consists of one Co atom, two Al atoms, and twelve O atoms (Co_I, Al_{II}, Al_{III}, O*n*, *n* = 1 to 12; see Fig. 1). The dotted blue lines are from both Co_I substituted and un-substituted surface layers; the dotted orange lines are the contribution from the Co_I substituted surface layer; the solid red lines are the contribution from d-type orbitals of Co_I; the solid brown lines are the contribution from s-type orbitals of Co_I.

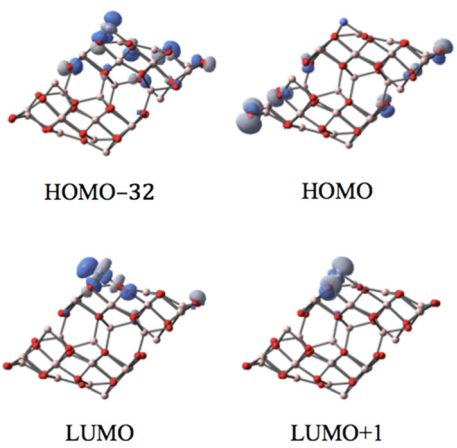

Fig. 3 The MOs associated with the band gap for the singlet state of the Co_I substituted $(111)_n$ surface of γ-alumina.

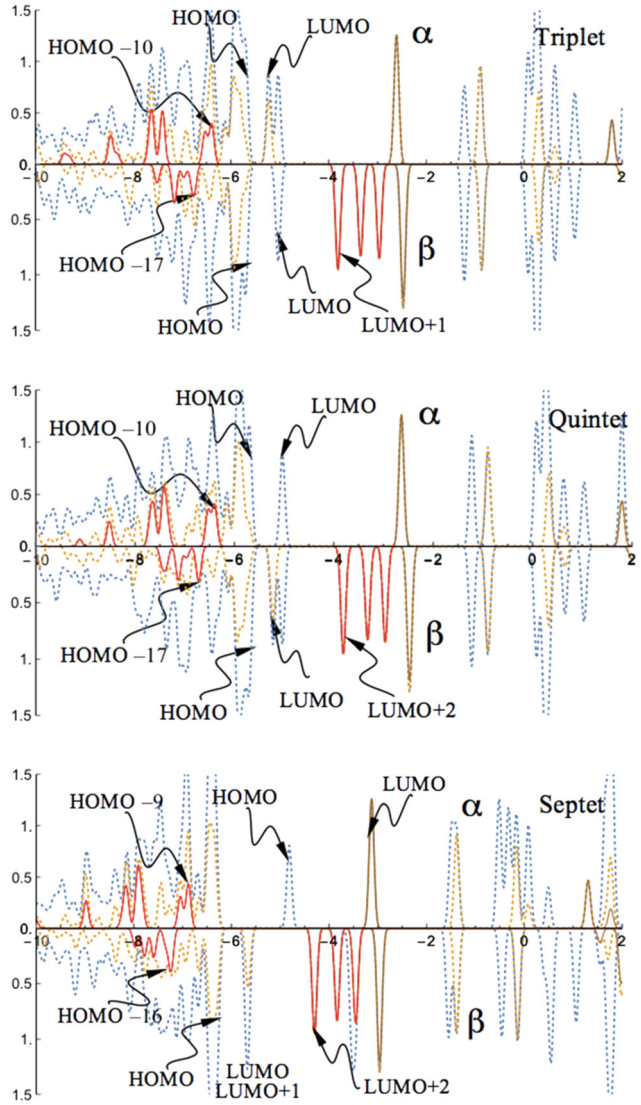

Fig. 4 PDOS of the Co_I substituted $(111)_n$ surface phase of γ-Al_2O_3 in the triplet, quintet, and septet states. The surface layer consists of one Co atom, two Al atoms, and twelve O atoms (Co_I, Al_{II}, Al_{III}, O*n*, *n* = 1 to 12; see Fig. 1). The dotted blue lines are from both Co_I substituted and un-substituted surface layers; the dotted orange lines are the contribution from the Co_I substituted surface layer; the solid red lines are the contribution from d-type orbitals of Co_I; the solid brown lines are the contribution from s-type orbitals of Co_I.

MOs of the septet state in Fig. 6 reveal the participation of s-orbital components of Al_I (HOMO) and Co_I (LUMO) in the large band gap in α-spin contributions.

Three well-localized d-orbitals of Co_I can be identified in the β-spin component as unoccupied orbitals for all high spin states. They are the LUMO+1, LUMO+2, and LUMO+3 for the triplet, LUMO+2, LUMO+3, and LUMO+4 for the quintet, and LUMO+2, LUMO+3, and LUMO+5 for the septet state. Thus, three d-orbitals of Co_I are only half-occupied. Consequently, the coordinated Co_I on the $(111)_n$ surface of γ-Al_2O_3 has the open-shell d^7 electron configuration in the high spin states.

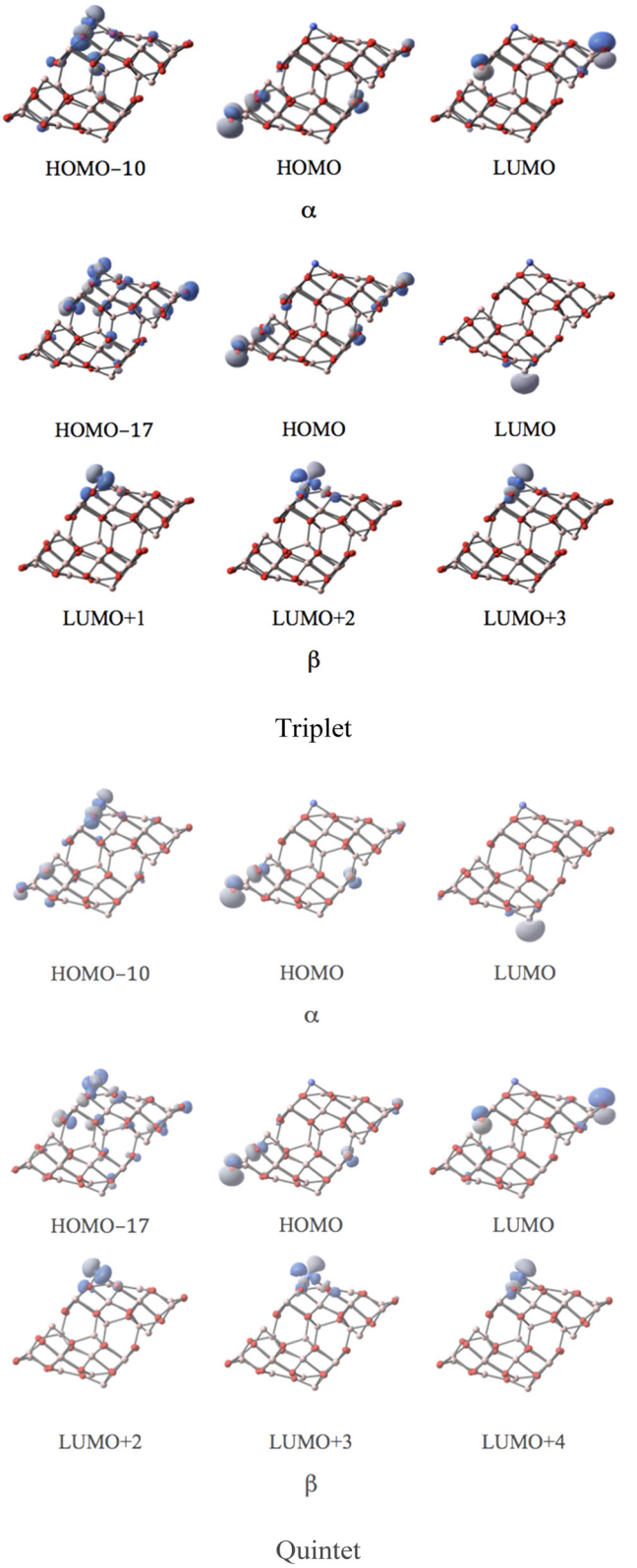

Fig. 5 The MOs associated with the band gap for the degenerate triplet and quintet states of the Co_I substituted $(111)_n$ surface of γ-alumina.

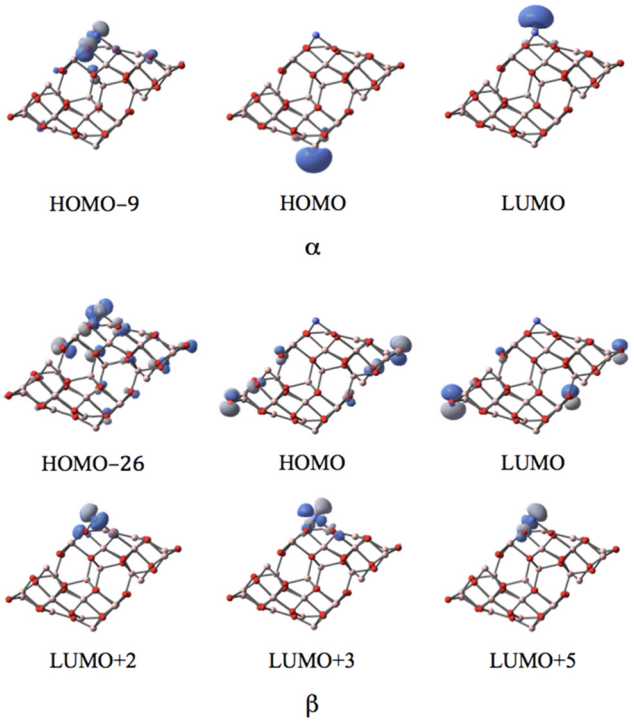

Fig. 6 The MOs associated with the band gap for the septet state of the Co_I substituted $(111)_n$ surface of γ-alumina.

2.2 Ni single site on the $(111)_n$ surface of γ-Al_2O_3

Three spin states were revealed for Ni on the substituted $(111)_n$ surface of γ-alumina, ranging from doublet (with $2S + 1 = 2$) to quartet ($2S + 1 = 4$) and sextet ($2S + 1 = 6$), respectively. The quartet is the ground state for the replacements of Ni on the Al_I site of the $(111)_n$ surface of γ-Al_2O_3. The energy released from the Ni substitution process Ni^{3+} (quartet) + [$(111)_n$ surface of γ-Al_2O_3] → Al^{3+} + [Ni_I (quartet) on the $(111)_n$ surface of γ-Al_2O_3] amounts to −164.85 kcal mol^{-1}, much larger than that in the corresponding Co substitution process (−113.17 kcal mol^{-1}) and in the corresponding Fe substitution (−44.30 kcal mol^{-1}). The details of relative stable energies of the Ni_I substituted surface $(111)_n$ of γ-Al_2O_3 with different spin states are provided in Table 4. It is clear that the doublet is virtually the same as the quartet state, in terms of energy. Thus, similar to the case of the Co_I complex, the ground state for the single Ni_I substituted $(111)_n$ surface of γ-Al_2O_3 is nearly degenerate. The predicted energy difference between ion Ni^{3+} (quartet, ground state) and ion Ni^{3+}(doublet) amounts to 30.49 kcal mol^{-1}. The degeneracy of the ground state of the γ-Al_2O_3 supported Ni_I complex implies that the coordination of the γ-Al_2O_3 surface may disturb its electron structure around the hosted Ni^{3+}.

Table 4 Relative energy of the Ni_I substituted surface $(111)_n$ of gamma alumina, optimized using the MN12-L functional with basis sets SV[a]

Site	Doublet	Quartet	Sextet
Ni_I	0.028	0.000	12.856

[a] For site labels, see Fig. 1. Relative energy in kcal mol^{-1}.

2.2.1 Local structure Ni_I site on the $(111)_n$ surface. The coordinates of the optimized structures of the Ni_I substituted $(111)_n$ surface of the supercell in doublet, quartet, and sextet are listed in the ESI.†

Table 5 summarizes the main geometric parameters of the optimized structure of the Ni_I substituted $(111)_n$ surface of γ-Al_2O_3. Replacement of Al_I by Ni on the $(111)_n$ surface leads to elongations of metal–O bond lengths as compared to the pure γ-Al_2O_3. The Ni_I–O distances amount to 1.90–1.91 Å for all three spin states of the Ni_I substituted $(111)_n$ complex, approximately 0.14 Å longer than the corresponding Al_I–O distance of the un-substituted $(111)_n$ surface. Consistent with the energetic degeneracy, nearly the same Ni_I–O bond lengths (~1.91 Å) are identified for both doublet and quartet states. A similar local structure is also unveiled for the system with the highest spin state. The related Ni_I–O distances are computed to be ~1.91 Å for the sextet state. The local geometric feature of the Ni_I substituted surface $(111)_n$ of gamma alumina resembles those of the Co_I substituted surface $(111)_n$ in high spin states (triplet, quintet, and septet). On the other hand, the structure corresponding to short Co_I–O and Fe_I–O distances (1.77–1.78 Å) for the low spin state of the Co_I and Fe_I substituted $(111)_n$ surface of γ-Al_2O_3 has not been revealed for the Ni_I substituted $(111)_n$ surface of γ-Al_2O_3.

2.2.2 Electron density distribution, DOS, and MO analysis of the Ni_I site. The effects of the substitution of Ni on the Al_I site on charge redistributions of the surrounding atoms have been revealed by the Mulliken population analysis (Table 6). The charge on the Ni_I atom is 1.46 au, approximately, for all the spin states. In comparison with Al_I (1.77 au), Ni_I has a smaller charge, about 0.31 au on the $(111)_n$ surface. Accordingly, the O atoms coordinated to Ni_I are expected to be less charged as compared to the non-substituted complex. The charge densities are calculated to be −1.193–−1.196 au on the O1 and −1.191–−1.194 au on the O2 atom, respectively. As a comparison, these charges amount to −1.216 au on the non-substituted surface. The charge density on O3 is −1.178–−1.183 au, larger by about −0.01 au in comparison with the non-substituted surface (−1.169 au for O3). It is important to note that the spin density distributions around the Ni_I site are similar among these three spin states: ~1.62 for Ni_I; ~0.10 to 0.11 for all three coordination O sites. Therefore, the variations of the total spin density do not alter the local electronic configuration of the Ni_I coordination site. Approximately, two spin electrons can be assigned to the Ni_I site, and one can be allocated on the neighboring O12 site of the surface layer (spin density of −0.72, β-spin in the doublet; 0.73, α-spin in the quartet and sextet). For the sextet state, one more spin electron is allocated on the un-substituted $(111)_n$ surface. This spin density distribution pattern resembles that of the Co_I substituted surface $(111)_n$ in the high spin states discussed above.

Table 5 Geometries of the local structure of the Ni_I substituted surface $(111)_n$ of gamma alumina, optimized using the MN12-L functional with basis sets SV[a]

	Non-substituted		Ni-substituted	
	Singlet	Doublet	Quartet	Sextet
RI-1	1.766	1.907 (1.778)	1.908 (1.906)	1.905 (1.942)
RI-2	1.767	1.901 (1.779)	1.910 (1.908)	1.906 (1.941)
RI-3	1.763	1.905 (1.812)	1.904 (1.908)	1.905 (1.947)
D1123	51.29	58.16 (53.74)	58.08 (58.52)	58.31 (58.51)

[a] RI-*i*: Ni–O atomic distance for substituted surfaces (Al–O atomic distance for non-substituted surface) in Å; D*ijkl*: dihedral angle in (°); for labels, see Fig. 1. The numbers in parentheses are those of the Fe_I substituted surface $(111)_n$ of gamma alumina, computed at the same level of theory.[30]

Table 6 Mulliken charge and spin density of the local structure of the Ni_I substituted surface $(111)_n$[a]

	Doublet		Quartet		Sextet	
	Charge	Spin	Charge	Spin	Charge	Spin
Ni_I	1.4581 (1.5595)	1.619 (1.067)	1.4574 (1.5769)	1.623 (3.489)	1.4592 (1.5455)	1.623 (3.692)
O1	−1.1930 (−1.0696)	0.110 (−0.015)	−1.1936 (−1.1466)	0.115 (0.057)	−1.1958 (−1.1857)	0.116 (0.073)
O2	−1.1908 (−1.0683)	0.110 (−0.015)	−1.1913 (−1.1800)	0.115 (0.122)	−1.1940 (−1.2098)	0.115 (0.091)
O3	−1.1778 (−1.1045)	0.100 (−0.023)	−1.1788 (−1.1660)	0.100 (0.066)	−1.1829 (−1.2107)	0.099 (0.091)
O12	−0.7999 (−1.1341)	−0.723 (−0.017)	−0.8026 (−1.0533)	0.725 (−0.244)	−0.7955 (−0.8082)	0.7322 (0.712)

[a] Analysis based on the density calculated using the MN12-L functional with basis set SV. For labels, see Fig. 1. The numbers in parentheses are those of the Fe_I substituted surface $(111)_n$, computed at the same level of theory.[30]

For comparison, the corresponding Mulliken charge and spin density of the Fe_I substituted surface $(111)_n$ are also listed in Table 6. In the Fe_I substituted complex, one spin electron is assigned to Fe_I in its doublet state, while more than three spin electrons are located on Fe_I in the related quartet and sextet states.[30] Moreover, only in its sextet state, the neighboring O12 site of the surface layer hosts roughly one spin electron (spin density of 0.72, α-spin).

The PDOSs of the doublet and quartet states demonstrate nearly the same band character of the coordinated Ni_I, as expected from their similar charge and spin density distributions and from their energy degeneracy. No contributions from the d- or s-orbitals of the γ-Al_2O_3 surface near the band gap are revealed for these two degenerate states (Fig. 7).

The state densities flanking the band gap are mainly determined by the p-orbitals of the O atoms in the surface layer and the sp^3-orbitals of Al of the un-substituted $(111)_n$ surface. The band gaps are evaluated to be 0.47 eV (α-spin) and 0.66 eV (β-spin) for the doublet state, and 0.65 eV (α-spin) and 0.46 eV (β-spin) for the quartet state, respectively. This band gap pattern of the Ni_I substituted surface $(111)_n$ is nearly the same as that of the Co_I substituted surface $(111)_n$ in the energy degenerate triplet and quintet spin states and hence, both Ni_I substituted and Co_I substituted systems have similar band gaps.

For the sextet state, the s-type orbital (4s) of Ni serves as the LUMO in the α-spin component, and therefore the band gap is expected to change. A large band gap, 2.06 eV, is found for the α-spin contribution in the sextet state. Meanwhile, for the β-spin component, the band gap is dominated by the p-orbitals of the O atoms in the surface layer and the band gap value amounts to 0.65 eV for the β-spin component.

MOs of the doublet and quartet states depicted in Fig. 8 reveal the high similarity between the nearly degenerate doublet and quartet states of the Ni_I substituted surface. The unique difference is revealed in the case of the corresponding LUMO. While the p-type orbital of O12 of the coordinated Ni_I represents the LUMO with α-spin in the doublet, in the quartet, it swaps the spin to form a β-spin LUMO. The former suggests that in the doublet state, the corresponding p-type orbital is occupied in its β-spin component (spin density of −0.72 in Mulliken population analysis; balancing 1.62 of spin density on Ni results in a total spin density of 1), In the quartet state, the α-spin component of the p-type orbital is occupied (spin density of 0.72), leaving the corresponding β-spin orbital un-occupied, This α–β electron flipping on the

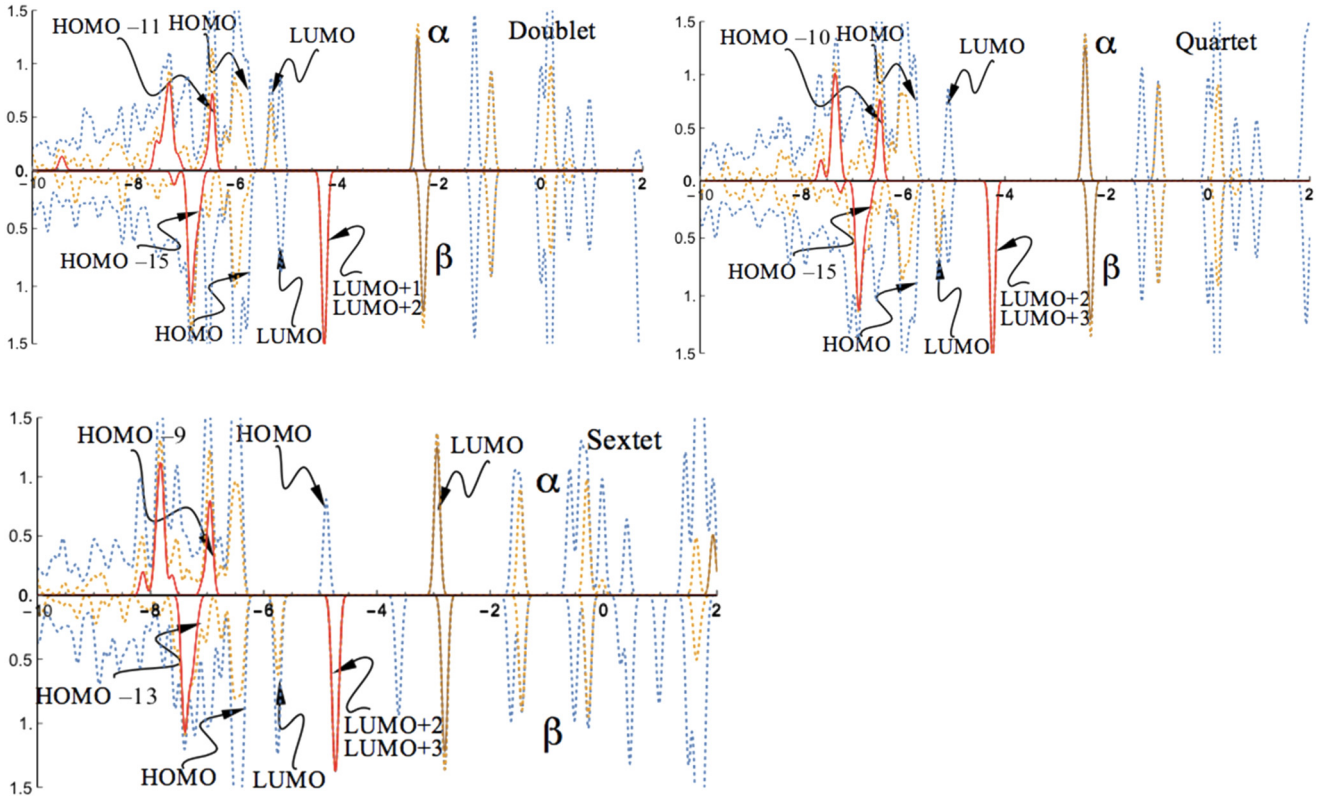

Fig. 7 PDOS of the Ni_I substituted $(111)_n$ surface phase of γ-Al_2O_3 in the doublet, quintet, and sextet states. The surface layer consists of one Ni atom, two Al atoms, and twelve O atoms (Ni_I, Al_{II}, Al_{III}, O*n*, *n* = 1 to 12; see Fig. 1). The dotted blue lines are from both Ni_I substituted and un-substituted surface layers; the dotted orange lines are the contribution from the Ni_I substituted surface layer; the solid red lines are the contribution from d-type orbitals of Ni_I; the solid brown lines are the contribution from s-type orbitals of Ni_I.

p-orbital of O12 leads to the energy degeneracy between the doublet and quartet states.

Five d-type orbitals of Ni_I are located below the HOMO−11 (ranging from HOMO−11 to HOMO−37) in the α-spin component for the doublet state, and below the HOMO−10 (ranging from HOMO−10 to HOMO−39) for the quartet state. In the β-spin state, only three d-orbitals of Ni_I can be identified below the HOMO−15 (ranging from HOMO−11 to HOMO−23) for the doublet state, and below the HOMO−15 (ranging from HOMO−10 to HOMO−24) for the quartet state. Two localized d-orbitals of Ni_I appear in the β-spin component as unoccupied orbitals for both doublet and quartet. These are the LUMO+1 and LUMO+2 in the doublet state, and the LUMO+2 and LUMO+3 in the quintet state. Consequently, the coordinated Ni_I on the $(111)_n$ surface of γ-Al_2O_3 has the open-shell d^8 electron configuration in the doublet and quartet spin states.

MOs of the sextet state in Fig. 9 reveal the participation of s-orbital components of Al_I (HOMO) and Ni_I (LUMO) in the large band gap in α-spin, which resembles the case of coordinated Co_I on the $(111)_n$ surface.

In the sextet state, five occupied d-type orbitals of Ni_I can be found below the HOMO−9 (ranging from HOMO−9 to HOMO−38) in the α-spin component. Meanwhile, three occupied d-orbitals of Ni_I can be identified below the HOMO −13 (ranging from HOMO−13 to HOMO−21) for the sextet state. Two unoccupied d-orbitals of Ni_I appear in the corresponding β-spin component (LUMO+2 and LUMO+3). Consequently, the coordinated Ni_I on the $(111)_n$ surface of γ-Al_2O_3 also has the open-shell d^8 electron configuration in the sextet spin state.

3 Conclusions

A computational study of coordination of Co and Ni single-atom sites on the most active tri-coordinated Al/metal single-site $(111)_n$ surface of γ-Al_2O_3 reveals that the energy released from the single atom substitution process on the Al_I site of $(111)_n$ surface follows the sequence Ni_I (164.85 kcal mol^{-1}) > Co_I (113.17 kcal mol^{-1}) > Fe_I (44.30 kcal mol^{-1}).

The ground states of both Co_I and Ni_I substituted single-site $(111)_n$ surfaces of γ-Al_2O_3 are energy degenerate. The triplet and quintet states of the Co_I substituted complex have the same stable energy. The same energy degeneracy is predicted for the doublet and quartet states of the Ni_I substituted complex. This arises from the α–β electron flipping on the p-orbital of the neighboring O12 that is next to the substituted transition metal site on the $(111)_n$ surface of γ-Al_2O_3. As shown in our previous study on the CO/CO_2 conversion mechanism on the calcium ferrite (CFO) surface,

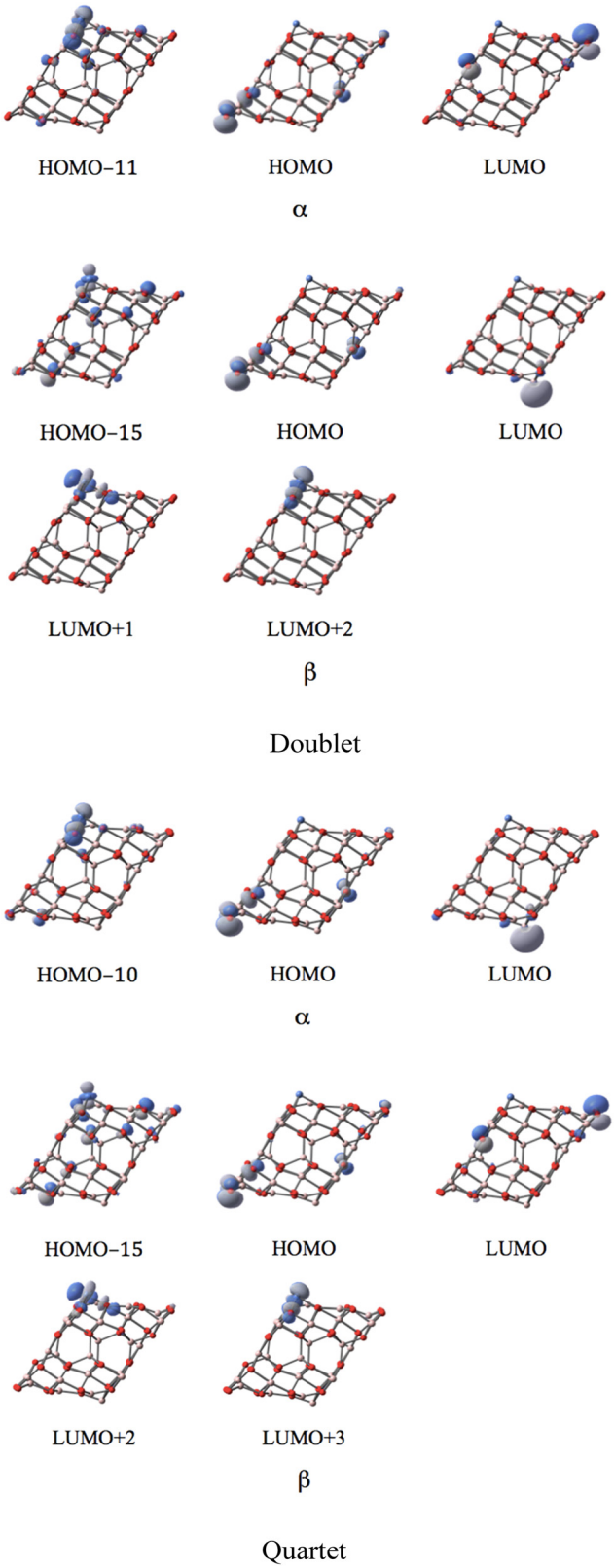

Fig. 8 The MOs associated with the band gap for the degenerate doublet and quartet states of the Ni_I substituted $(111)_n$ surface of γ-alumina.

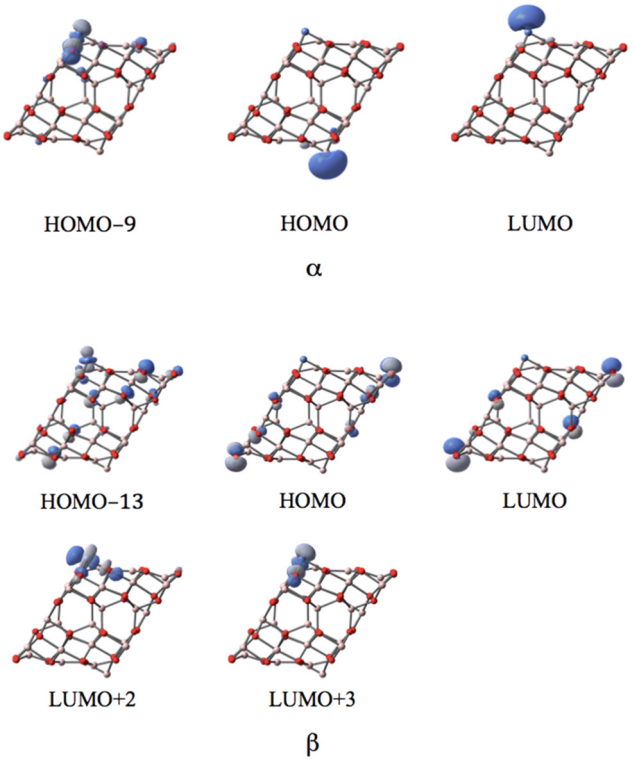

Fig. 9 The MOs associated with the band gap for the sextet state of the Ni_I substituted $(111)_n$ surface of γ-alumina.

these energy degenerate Co_I or Ni_I sites on the $(111)_n$ surface of γ-Al_2O_3 could serve as effective catalytic centers for the CO/CO_2 conversion.

Different from the Fe_I substituted single-site $(111)_n$ surface, in which the electron configuration of Fe_I varies according to its spin-multiplicity state, Ni_I has a unique d^8 electron configuration in all three spin states of the Ni_I substituted single-site $(111)_n$ surface. Analogously, Co_I has a unique d^7 electron configuration in all three open shell spin states of the Co_I substituted single-site $(111)_n$ surface. Only in the singlet state, Co_I adopts a d^6 electron configuration on the supportive $(111)_n$ surface of γ-Al_2O_3. Consequently, in the state with the highest spin multiplicity, the spin density extends to the un-substituted $(111)_n$ surface for the Co_I and Ni_I substituted single-site $(111)_n$ systems. In contrast, in the case of Fe substitution, the change of spin multiplicity only leads to the alternation of the electron configuration of Fe_I, and the spin density distribution is limited to the Fe_I substituted site and its close neighboring O on the substituted surface.

The replacement of Al by a Co or Ni atom on the I position of the $(111)_n$ surface leads to significant elongations of metal–O distances. Different from the Fe_I substitution case, these atomic distance elongations are less affected by the variation of the corresponding spin-multiplicity states of Co_I and Ni_I. This is due to the unique d-electron configuration of the substituted Co_I (d^7) and Ni_I (d^8) atoms at the surface site. Thus, an increase of d-electrons (compared

to the case of iron atom) on the metal substituted $(111)_n$ surface of γ-Al_2O_3 results in the formation of stable local structures and steady d-electron configurations for the Co_I and Ni_I substituted complexes. A previous study indicated that the most stable Fe_I adopts a d^5 electron configuration,[30] so one might expect a d^6 and d^7 electron configuration for the Co_I and Ni_I complexes, respectively. However, the present study illustrates that by increasing the number of d-electrons by one and two, the most stable electron configuration becomes d^7 for Co_I and d^8 for Ni_I. It is interesting to understand the effects of reducing the number of d-electrons on the Fe_I substituted $(111)_n$ surface of γ-Al_2O_3, as is the case in the Cr_I and Mn_I substituted surface systems. These systems are currently studied in our laboratory.

4 Methods of computation

The DFT method along with the functional by Peverati and Truhlar (MN12-L)[55] has been used in the present study. Different from traditional surface studies using the plane wave basis such as in the Vienna *ab initio* simulation package (VASP),[56,57] here the localized basis set, namely the split valence basis set SV by Ahlrichs and coworkers,[58] was applied. Reasonable estimations of the cell volume were achieved using the MN12-L functional (with double and triple zeta basis sets, *i.e.* SV and TZV) as reported in our previous studies.[29,30,44] Compared to the experimental value of the cell volume of 46.39 ($Å^3/Al_2O_3$), a cell volume of 46.94 ($Å^3/Al_2O_3$) calculated at the MN12-L/SV level with the PBC approach is better than the VASP result of 47.40 ($Å^3/Al_2O_3$).[29,30,44] It is important to note that the application of 2-dimensional periodic boundary conditions implies an infinite vacuum above the studied surface. Therefore, the artificial long-range interactions between the surfaces are excluded by this method. The application of the MN12-L functional is an efficient approach for the computational investigation of gamma alumina systems. As a reliable compromise between accurateness and computational feasibility, the MN12-L/SV approach is applied in the reported calculations. Periodic boundary conditions were applied for the description of the bulk phase. The total *k*-point numbers amount to 4 × 6 × 6 (for the supercell) for the bulk phase. For the computations of the surface phases, 2-dimensional periodic boundary conditions were applied. The total *k*-point number is 10 × 10 in the surface phase computations. For the study of the surface, the positions of all of the atoms were fully optimized while the corresponding lattice vectors were kept fixed. It is important to note that application of 2-dimensional periodic boundary conditions implies an infinite vacuum above the studied surface. Therefore, the artificial long-range interactions between the surfaces are excluded by this method. The Gaussian-09 package of programs[59] was applied for all computations.

The hexagonal cell unit model described in our previous study (ref. 30 and 44, consisting of $(111)_n$, (100) and (110) planes) was adapted in the present investigation of the $(111)_n$ surface. To ensure that there is a sufficient bulk environment underneath the investigated surface, a supercell model consisting of two units along the $(111)_n$ surface direction (8 atomic slabs) has been adapted (see Fig. 1).

Conflicts of interest

The authors declare no conflict of interest.

Acknowledgements

This study was supported by the NSF PREM grant #1826886. The computer time was provided by the Extreme Science and Engineering Discovery Environment (XSEDE) by the National Science Foundation Grant Number OCI-1053575 and XSEDE award allocation number DMR110088 and by the Mississippi Center for Supercomputer Research.

References

1 L. L. Liu and A. Corma, Metal catalysts for heterogeneous catalysis: from single atoms to nanoclusters and nanoparticles, *Chem. Rev.*, 2018, **118**, 4981–5079.
2 C. S. Maldonado, J. R. De la Rosa, C. J. Lucio-Ortiz, A. Hernández-Ramírez, F. F. C. Barraza and J. S. Valente, Low concentration Fe-doped alumina catalysts using sol-gel and impregnation methods: the synthesis, characterization and catalytic performance during the combustion of trichloroethylene, *Materials*, 2014, **7**, 2062–2086.
3 S. Mosallanejad, B. Z. Dlugogorski, E. M. Kennedy and M. Stockenhuber, On the chemistry of iron oxide supported on γ-alumina and silica catalysts, *ACS Omega*, 2018, **3**, 5362–5374.
4 T. Yang, R. Fukuda, S. Hosokawa, T. Tanaka, S. Sakaki and M. Ehara, A theoretical investigation on CO oxidation by single-atom catalysts M1/γ-Al_2O_3 (M=Pd, Fe, Co, and Ni), *ChemCatChem*, 2017, **9**, 1222–1229.
5 J. Wang, J. Gu, A. Rony, M. Fan and J. Leszczynski, Theoretical DFT study on the mechanisms of CO/CO_2 conversion in chemical looping catalyzed by calcium ferrite, *J. Phys. Chem. A*, 2021, **125**, 8159–8167.
6 Q. Fu, W.-X. Li, Y. Yao, H. Liu, H.-Y. Su, D. Ma, X.-K. Gu, L. Chen, Z. Wang, H. Zhang, B. Wang and X. Bao, Interface-confined ferrous centers for catalytic oxidation, *Science*, 2010, **328**, 1141–1144.
7 M. Haruta, Size- and support-dependency in the catalysis of gold, *Catal. Today*, 1997, **36**, 153–166.
8 B. Qiao, J.-X. Liang, A. Wang, C.-Q. Xu, J. Li, T. Zhang and J. J. Liu, Ultrastable single-atom gold catalysts with strong covalent metal- support interaction (CMSI), *Nano Res.*, 2015, **8**, 2913–2924.
9 B. Qiao, J. Liu, Y.-G. Wang, Q. Lin, X. Liu, A. Wang, J. Li, T. Zhang and J. Liu, Highly efficient catalysis of preferential oxidation of CO in H-rich stream by gold single-atom catalysts, *ACS Catal.*, 2015, **25**, 6249–6254.
10 B. Qiao, A. Wang, X. Yang, L. F. Allard, Z. Jiang, Y. Cui, J. Liu, J. Li and T. Zhang, Single-atom catalysis of CO oxidation using Pt_1/ FeOx, *Nat. Chem.*, 2011, **3**, 634–641.

11 M. Moses-DeBusk, M. Yoon, L. F. Allard, D. R. Mullins, Z. Wu, X. Yang, G. Veith, G. M. Stocks and C. K. Narula, CO oxidation on supported single Pt atoms: experimental and ab initio density functional studies of CO interaction with Pt atom on θ-Al_2O_3(010) surface, *J. Am. Chem. Soc.*, 2013, **135**, 12634–12645.

12 L. DeRita, S. Dai, K. Lopez-Zepeda, N. Pham, G. W. Graham, X. Pan and P. Christopher, Catalyst architecture for stable single atom dispersion enables site-specific spectroscopic and reactivity measure- ments of CO adsorbed to Pt atoms, oxidized Pt clusters, and metallic Pt clusters on TiO_2, *J. Am. Chem. Soc.*, 2017, **139**, 14150–14165.

13 J. D. Kistler, N. Chotigkrai, P. Xu, B. Enderle, P. Praserthdam, C. Y. Chen, N. D. Browning and B. C. Gates, A single-site platinum CO oxidation catalyst in zeolite KLTL: microscopic and spectroscopic determination of the locations of the platinum atoms, *Angew. Chem., Int. Ed.*, 2014, **53**, 8904–8907.

14 J. Saavedra, T. Whittaker, Z. Chen, C. J. Pursell, R. M. Rioux and B. D. Chandler, Controlling activity and selectivity using water in the Au-catalysed preferential oxidation of CO in H_2, *Nat. Chem.*, 2016, **8**, 584–589.

15 J. Jones, H. Xiong, A. T. DeLaRiva, E. J. Peterson, H. Pham, S. R. Challa, G. Qi, S. Oh, M. H. Wiebenga, X. I. Pereira Hernandez, Y. Wang and A. K. Datye, Thermally stable single-atom platinum-on-ceria catalysts via atom trapping, *Science*, 2016, **353**, 150–154.

16 Z. Zhang, Y. Zhu, H. Asakura, B. Zhang, J. Zhang, M. Zhou, Y. Han, T. Tanaka, A. Wang and T. Zhang, Thermally stable single atom Pt/m-Al_2O_3 for selective hydrogenation and CO oxidation, *Nat. Commun.*, 2017, **8**, 16100.

17 E. J. Peterson, A. T. DeLaRiva, S. Lin, R. S. Johnson, H. Guo, J. T. Miller, J. Hun Kwak, C. H. Peden, B. Kiefer, L. F. Allard, F. H. Ribeiro and A. K. Datye, Low-temperature carbon monoxide oxidation catalysed by regenerable atomically dispersed palladium on alumina, *Nat. Commun.*, 2014, **5**, 4885.

18 X.-K. Gu, B. Qiao, C.-Q. Huang, W.-C. Ding, K. Sun, E. Zhan, T. Zhang, J. Liu and W.-X. Li, Supported single Pt_1/Au_1 atoms for methanol steam reforming, *ACS Catal.*, 2014, **4**, 3886–3890.

19 Y. Zhu, A. An and J. He, Single-atom and small-cluster Pt induced by Sn (IV) sites confined in an LDH lattice for catalytic reforming, *J. Catal.*, 2016, **341**, 44–54.

20 S. De, B. Saha and R. Luque, Hydrodeoxygenation processes: advances on catalytic transformations of biomass-derived platform chemicals into hydrocarbon fuels, *Bioresour. Technol.*, 2015, **178**, 108–118.

21 X. Guo, G. Fang, G. Li, H. Ma, H. Fan, L. Yu, C. Ma, X. Wu, D. Deng and M. Wei, Direct, nonoxidative conversion of methane to ethylene, aromatics, and hydrogen, *Science*, 2014, **344**, 616–619.

22 H. Duan, M. Li, G. Zhang, J. R. Gallagher, Z. Huang, Y. Sun, Z. Luo, H. Chen, J. T. Miller and R. Zou, Single-site palladium(II) catalyst for oxidative heck reaction: catalytic performance and kinetic investigations, *ACS Catal.*, 2015, **5**, 3752–3759.

23 E. D. Metzger, C. K. Brozek, R. J. Comito and M. Dinca, Selective dimerization of ethylene to 1-butene with a porous catalyst, *ACS Cent. Sci.*, 2016, **2**, 148–153.

24 S. K. Kaiser, Z. Chen, D. F. Akl, S. Mitchell and J. Peŕez-Ramírez, Single-atom catalysts across the periodic table, *Chem. Rev.*, 2020, **120**, 11703–11809.

25 R. Wisechert, P. Florian, C. Copéret, D. Massiot and P. Sautet, Visibility of Al surface sites of γ-alumina: a combined computational and experimental point of view, *J. Phys. Chem. C*, 2014, **118**, 15292–15299.

26 J. H. Kwak, D. Mei, C. H. F. Peden, R. Rousseau and J. Szanyi, (100) Facets of γ- Al_2O_3: the active surfaces for alcohol dehydration reactions, *Catal. Lett.*, 2011, **141**, 649–655.

27 J. H. Kwak, J. Hu, D. Mei, C.-W. Yi, D. H. Kim, C. H. F. Peden, L. F. Allard and J. Szanyi, Coordinatively unsaturated Al^{3+} centers as binding sites for active catalyst phases of platinum on γ- Al_2O_3, *Science*, 2009, **325**, 1670–1673.

28 J. R. Copeland, X.-R. Shi, D. S. Sholl and C. Sievers, Surface interactions of C_2 and C_3 polyols with γ-Al_2O_3 and the role of Co-adsorbed water, *Langmuir*, 2012, **29**, 581–593.

29 J. Gu, J. Wang and J. Leszczynski, Single site Fe on the (110) surface of γ-Al_2O_3: insights from a DFT study including the periodic boundary approach, *Phys. Chem. Chem. Phys.*, 2021, **23**, 7164–7177.

30 J. Gu, J. Wang and J. Leszczynski, Single Fe site on the surface of γ-Al_2O_3: insights from density functional theory periodic boundary approach, *J. Phys. Chem. C*, 2020, **124**, 20931–20941.

31 S. J. Wilson, The dehydration of boehmite, γ-AlOOH, to γ-Al_2O_3, *J. Solid State Chem.*, 1979, **30**, 247–255.

32 R. Goswami, C. S. Pande, N. Bernstein, M. D. Johannes, C. Baker and G. Villalobos, A high degree of enhancement of strength of sputter deposited Al/Al_2O_3 multilayers upon post annealing, *Acta Mater.*, 2015, **95**, 378–385.

33 M. Digne, P. Sautet, P. Raybaud, P. Euzen and H. Toulhoat, Use of DFT to achieve a rational understanding of acid–basic properties of γ-alumina surfaces, *J. Catal.*, 2004, **226**, 54–68.

34 M. Digne, P. Sautet, P. Raybaud, P. Euzen and H. Toulhoat, Hydroxyl groups on γ-alumina surfaces: a DFT study, *J. Catal.*, 2002, **211**, 1–5.

35 H. P. Pinto, R. M. Nieminen and S. D. Elliott, Ab initio study of γ–Al_2O_3 surfaces, *Phys. Rev. B: Condens. Matter Mater. Phys.*, 2004, **70**, 125402.

36 L. Kovarik, A. Genc, C. Wang, A. Qiu, C. H. F. Peden, J. Szanyi and J. H. Kwak, Tomography and high-resolution electron microscopy study of surfaces and porosity in a plate-like γ-Al_2O_3, *J. Phys. Chem. C*, 2013, **117**, 179–186.

37 R. Wisechert, C. Copéret, F. Delbecq and P. Sautet, Optimal water coverage on alumina: a key to generate lewis acid–base pairs that are reactive towards the C—H bond activation of methane, *Angew. Chem., Int. Ed.*, 2011, **50**, 3202–3205.

38 J. G. Larson and W. K. Hall, Studies of the hydrogen held by solids. VII. the exchange of the hydroxyl groups of alumina and silica-alumina catalysts with deuterated methane, *J. Phys. Chem.*, 1965, **69**, 3080–3089.

39 P. J. Robertson, M. S. Scurrell and C. Kemball, Exchange of alkanes with deuterium over γ-alumina. aBrønsted linear free energy relationship, *J. Chem. Soc., Faraday Trans.*, 1975, **71**, 903–912.

40 J. S. J. Hargreaves, G. J. Hutchings, R. W. Joyner and S. H. Taylor, A study of the methane–deuterium exchange reaction over a range of metal oxides, *Appl. Catal., A*, 2002, **227**, 191–200.

41 L. Quanzhi and Y. Amenomiya, Exchange reaction of methane on some oxide catalysts, *Appl. Catal.*, 1986, **23**, 173–182.

42 H. Knozinger and P. Ratnasamy, Catalytic aluminas: surface models and characterization of surface sites, *Catal. Rev.: Sci. Eng.*, 1978, **17**, 31–70.

43 J. Joubert, A. Salameh, V. Krakoviack, F. Delbecq, P. Sautet, C. Coperet and J.-M. Basset, Heterolytic splitting of H_2 and CH_4 on γ-alumina as a structural probe for defect sites, *J. Phys. Chem. B*, 2006, **110**, 23944–23950.

44 J. Gu, J. Wang and J. Leszczynski, Structure and energetics of (111) surface of γ-Al_2O_3: insights from DFT including periodic boundary approach, *ACS Omega*, 2018, **3**, 1881–1888.

45 S. Zhang, L. Nguyen, J.-X. Liang, J. Shan, J. Liu, A. I. Frenkel, A. Patlolla, W. Huang, J. Li and F. Tao, Catalysis on singly dispersed bimetallic sites, *Nat. Commun.*, 2015, **6**, 7938.

46 L. Nguyen, S. Zhang, L. Wang, Y. Li, H. Yoshida, A. Patlolla, S. Takeda, A. I. Frenkel and F. Tao, Reduction of nitric oxide with hydrogen on catalysts of singly dispersed bimetallic sites Pt_1Co_m and Pd_1Co_n, *ACS Catal.*, 2016, **6**, 840–850.

47 Y. Han, Y.-G. Wang, W. Chen, R. Xu, L. R. Zheng, J. Zhang, J. Luo, R.-A. Shen, Y. Zhu and W.-C. Cheong, Hollow N-doped carbon spheres with isolated cobalt single atomic sites: superior electrocatalysts for oxygen reduction, *J. Am. Chem. Soc.*, 2017, **139**, 17269–17272.

48 P. Yin, T. Yao, Y. Wu, L. Zheng, Y. Lin, W. Liu, H. Ju, J. Zhu, X. Hong and Z. Deng, Single cobalt atoms with precise N-coordination as superior oxygen reduction reaction catalysts, *Angew. Chem., Int. Ed.*, 2016, **55**, 10800–10805.

49 Q. Cheng, L. Yang, L. Zou, Z. Zou, C. Chen, Z. Hu and H. Yang, Single cobalt atom and N codoped carbon nanofibers as highly durable electrocatalyst for oxygen reduction reaction, *ACS Catal.*, 2017, **7**, 6864–6871.

50 Y. Zheng, Y. Jiao, Y. Zhu, Q. Cai, A. Vasileff, L. H. Li, Y. Han, Y. Chen and S. Z. Qiao, Molecule-level g-C_3N_4 coordinated transition metals as a new class of electrocatalysts for oxygen electrode reactions, *J. Am. Chem. Soc.*, 2017, **139**, 3336–3339.

51 Y. Chen, S. Ji, Y. Wang, J. Dong, W. Chen, Z. Li, R. Shen, L. Zheng, Z. Zhuang and D. Wang, Isolated single iron atoms anchored on N-doped porous carbon as an efficient electrocatalyst for the oxygen reduction reaction, *Angew. Chem., Int. Ed.*, 2017, **56**, 6937–6941.

52 H. T. Chung, D. A. Cullen, D. Higgins, B. T. Sneed, E. F. Holby, K. L. More and P. Zelenay, Direct atomic-level insight into the active sites of a high-performance PGM-free ORR catalyst, *Science*, 2017, **357**, 479–484.

53 C. Zhu, S. Fu, J. Song, Q. Shi, D. Su, M. H. Engelhard, X. Li, D. Xiao, D. Li and L. Estevez, Self-assembled Fe-N-doped carbon nanotube aerogels with single-atom catalyst feature as high- efficiency oxygen reduction electrocatalysts, *Small*, 2017, **13**, 1603407.

54 Z. Zhang, X. Gao, M. Dou, J. Ji and F. Wang, Biomass derived N-doped porous carbon supported single Fe atoms as superior electrocatalysts for oxygen reduction, *Small*, 2017, **13**, 1604290.

55 R. Peverati and D. G. Truhlar, An improved and broadly accurate local approximation to the exchange–correlation density functional: the MN12-L functional for electronic structure calculations in chemistry and physics, *Phys. Chem. Chem. Phys.*, 2012, **10**, 13171–13174.

56 G. Kresse and D. Joubert, From ultrasoft pseudopotentials to the projector augmented-wave method, *Phys. Rev. B: Condens. Matter Mater. Phys.*, 1999, **59**, 1758–1775.

57 G. Kresse and J. Furthmüller, Efficient iterative schemes for ab initio total-energy calculations using a plane-wave basis set, *Phys. Rev. B: Condens. Matter Mater. Phys.*, 1996, **54**, 11169–11186.

58 A. Schaefer, H. Horn and R. Ahlrichs, Fully optimized contracted Gaussian-basis sets for atoms Li to Kr, *J. Chem. Phys.*, 1992, **97**, 2571–2577.

59 M. J. Frisch, G. W. Trucks, H. B. Schlegel, M. A. Scuseria, J. R. Robb, G. Cheeseman, V. Scalmani, B. Barone, G. A. Mennucci and G. E. Petersson, *Gaussian 09, Revision D.01*, Gaussian, Inc., Wallingford CT, 2009.